

Instability of QBC systems to Topological Anderson Insulating phases

Nicolau Sobrosa¹, Miguel Gonçalves², Eduardo V. Castro^{1,3}

¹*Centro de Física das Universidades do Minho e Porto,
Departamento de Física e Astronomia, Faculdade de Ciências,
Universidade do Porto, 4169-007 Porto, Portugal*

²*CeFEMA, Instituto Superior Técnico, Universidade de Lisboa,
Av. Rovisco Pais, 1049-001 Lisboa, Portugal and*

³*Beijing Computational Science Research Center, Beijing 100084, China*

Here we study the instabilities of a quadratic band crossing system to Chern insulating states and uncorrelated disorder. We determined the phase diagram in the plane of topological mass versus disorder strength, characterizing the system with respect to spectral, localization and topological properties. In the clean limit, the system has two gapped Chern insulating phases with Chern numbers $C = \pm 2$, and a trivial phase with $C = 0$. For finite disorder, the quadratic band crossing points are unstable to emergent gapless Chern insulating phases with $C = \pm 1$, not present in the clean limit. These phases occupy a considerable region of the phase diagram for intermediate disorder and show features of topological Anderson insulators: it is possible to reach them through disorder-driven transitions from trivial phases.

I. INTRODUCTION

Topological insulators are a remarkable state of electronic matter. They show quantized responses that are proportional to topological invariants and, as a consequence, typically very robust to perturbations and system's details [1–4]. Topological band insulators, as paradigmatic examples of systems with non-trivial topology, have been extensively studied and are fairly well understood [3]. Non-trivial topology however also manifests in systems with broken translational invariance that are not described by topological band theory. Among these systems, disordered topological insulators are a popular sub-group [5].

Topological phases are robust to disorder regarding that no symmetry protecting the topological properties is broken [6, 7]. In quantum Hall insulators, disorder even plays a fundamental role for the observation of a quantized Hall conductance. In the case of Chern insulators where time-reversal symmetry is broken, disorder localizes every eigenstate except at specific energies [8–12]. The extended eigenstates at these energies carry finite Chern numbers and are therefore responsible for a quantized Hall response as long as the Fermi level lies between them (the localized states cannot change this response). Topological phase transitions in disordered Chern insulators occur when the extended states merge and annihilate at the Fermi level (through the so-called “levitation and annihilation” mechanism), becoming localized [10].

Quite surprisingly, in some systems topological phase transitions between trivial and topological phases can occur by increasing disorder. These disorder-driven topological phases are now known as topological Anderson insulators (TAI) [13, 14]. This phase has been observed in many models, including paradigmatic models of topological insulators in two-dimensions (2D) such as the Kane-Mele model [15, 16] and the disordered Haldane model

[17–19].

Systems with quadratic band crossings (QBC) in 2D are also very interesting because, contrary to conventional band degeneracy points, they are associated with a finite Berry phase of $\pm 2\pi$. Due to the finite density of states at QBC, these systems are unstable to interactions [20]: originating nematic phases with two Dirac cones, each carrying half of the QBC's Berry phase; or gap openings that may give rise to topological insulating phases precisely due to the non-trivial Berry phase of the QBC [21–24]. The fate of interaction induced topological insulating phases in the presence of disorder has been examined in Refs. [25, 26] within the one-loop RG approach. The suppression of topological phases under increasing disorder and possible transition to trivial phases was predicted.

In this work we study the interplay between the instability of a QBC system to a Chern insulating state and to disorder of the Anderson type. The full phase diagram in the plane of the gap opening coupling parameter B and disorder strength W is shown in Fig. 1. For null disorder, QBC points (QBCP) occur for $B = -2, 0$, otherwise, the system is a gapped trivial insulator or a Chern insulator with Chern number $C = \pm 2$. These phases are also present for finite disorder, but new gapless Chern insulating phases also emerge. Besides gapless and gapped phases with $C = \pm 2$, new gapless topological phases with $C = \pm 1$, not present in the clean limit, arise. In fact, the most important result of our work is that the QBCP are unstable to the formation of these phases, for any finite disorder. Finally, the existence of TAI phenomena is also clear: it is possible to undergo a transition between the trivial phase and the disorder-induced topological phases with $C = \pm 1$ by increasing disorder.

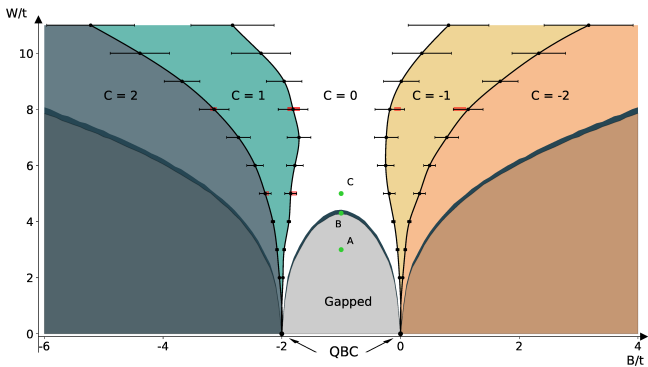


FIG. 1. Phase diagram in the $B-W$ plane. The Chern number was calculated for a system with 35×35 lattice points and was averaged for 100 disorder realizations. The gray areas correspond to the gapped regions obtained through calculations of the DOS. The error bars for the Chern number were obtained by fixing the disorder intensity and varying B . The red boxes indicate the results for the critical points calculated with the TMM. The size of the bar is determined in such a way that outside them the system is clearly localized (Λ_M decreases with M , see Fig. 5).

II. MODEL AND METHODS

We study a QBCP system realized in the square lattice with two orbitals per site. The model considers first-neighbor hoppings between the same orbitals and second-neighbors hoppings connecting different orbitals. The Hamiltonian for the disorder-free model can be written in the reciprocal space as

$$H_0 = \sum_{\mathbf{k}} \Psi_{\mathbf{k}}^\dagger \mathcal{H}_{\mathbf{k}} \Psi_{\mathbf{k}}, \quad (1)$$

where $\Psi_{\mathbf{k}} = (|1, \mathbf{k}\rangle, |2, \mathbf{k}\rangle)$ is the two component spinor of the two orbitals and

$$\mathcal{H}_{\mathbf{k}} = \mathbf{h} \cdot \boldsymbol{\sigma}, \quad (2)$$

with $\boldsymbol{\sigma}$ the Pauli vector and the vector \mathbf{h} given by:

$$\begin{aligned} h_x &= 2t_x \sin k_x \sin k_y \\ h_y &= 0 \\ h_z &= t_z (\cos k_x - \cos k_y). \end{aligned} \quad (3)$$

In the following, we set $t_x = t_z = t$ and t to unity.

This model has two QBCP: at $\Gamma = (0, 0)$ and $M = (\pm\pi, \pm\pi)$. The term h_y is necessarily zero for a QBCP to exist. It is possible to break time-reversal symmetry by adding a finite h_y , that also opens a gap. For a constant h_y , the system is a trivial insulator. Similarly to the Haldane Model [27] we add a k -dependent component which allows us to tune independently the gap at each

QBCP. We used a simple choice that is dependent of a unique parameter, B :

$$h_y = 1 + \frac{B+1}{2} (\cos k_x + \cos k_y). \quad (4)$$

In real-space, the constant term corresponds to a intra-cell complex hopping between different orbitals and the term with k -modulation to a nearest neighbor complex hopping between different orbitals. As the modification in Eq. 4 does not change h_x and h_z , a QBCP still exists when $h_y = 0$ as seen before. For $B = 0$, there is a QBCP at M and for $B = -2$, there is a QBCP at Γ .

The disorder potential is easily added through:

$$H = H_0 + \sum_i \xi_i \hat{c}_i^\dagger \hat{c}_i, \quad (5)$$

where ξ_i are site-dependent potentials that follow the uniform distribution,

$$P_W(\xi_i) = \frac{1}{W} \Theta \left(\left| \xi_i \right| - \frac{W}{2} \right), \quad (6)$$

where W defines the disorder strength.

We carried out a complete study of the phase diagram of the model in Eq. 5, characterizing spectral, topological and localization properties. The density of states (DOS) was calculated for finite systems containing more than 10^6 sites using the Kite quantum transport software that has a very efficient implementation of the kernel polynomial method (KPM) [28]. The topological phase diagram was obtained by computing the Chern number through the Coupling Matrix Method introduced in Ref. [29]. The localization properties were characterized through the Transfer Matrix Method [30–32], that also allowed to cross-check the Chern number results. This method considers a finite system with a large longitudinal width L and a transverse length M which we varied in order to find the localization length in terms of M , λ_M . With the goal of obtaining the localization properties we studied the normalized localization length, $\Lambda_M = \lambda_M/M$, in the following way: if Λ_M decreases with M the states are localized in the thermodynamic limit which correspond to a insulating behaviour; on the other hand, if Λ_M increases with M the states are extended. Finally, a constant Λ_M is characteristic of critical states that appear at transition points between different phases. We choose L in order to obtain λ_M with less than 1% error. It is clear that the behaviour of Λ_M can capture topological phase transitions at finite disorder. As mentioned in the introduction, the spectrum of finite-disorder Chern insulators consists of localized states, except at specific energies where extended critical states live. Topological phase transitions occur

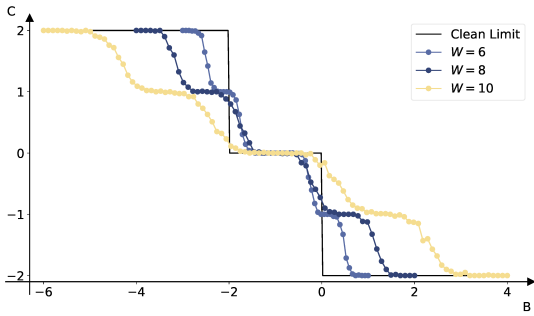


FIG. 2. Chern number results obtained at fixed W and variable B . The results were averaged over 120 disorder realizations. Each color depicts three examples of disorder intensities used. The full black curve represents the topological phases of the system calculated for null disorder where it is very clear that no $C = \pm 1$ phases exist.

when these states cross (and merge at) the Fermi level. Therefore, for a disordered Chern insulator, Λ_M should always decrease with M except at the topological phase transitions, where it becomes M -independent.

III. RESULTS

A. Topological Properties

In this section we present details on the topological phase diagram of Fig. 1. The different colors indicate different Chern Numbers and the black lines represent the topological transitions. For null disorder the system undergoes a transition from $C = \pm 2$ to $C = 0$ at the points where a QBCP appears. For finite disorder, the phases with $C = 0, \pm 2$ survive and a new gapless phase with $C = \pm 1$ appears. The latter phases are TAI as it is possible to reach them by increasing disorder from a topologically trivial phase, at fixed B . For large enough disorder, all topological phases are suppressed, in agreement with one-loop RG calculations [25].

To obtain the transition lines, W was fixed at some value and B was varied continuously. For each disorder strength we performed an average over 120 different disorder configurations with 35×35 sites. Some examples of the obtained curves are represented in the Fig. 2 including the values for the clean limit. The continuous variation of the chern number is expected to disappear in the thermodynamic limit, where transitions between different Chern numbers should become sharp. The errors that appear in Fig. 1 are determined by the curves of the Fig. 2. The error bars were considered to be the range over which the Chern number was more than 5% away from its integer value.

It is not clear from the phase diagram in Fig. 1 if the

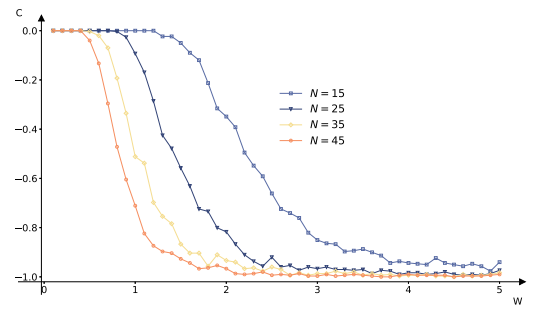


FIG. 3. Topological phases as function of disorder for $B = 0$ (QBC at $W = 0$) and variable system sizes with N unit cells in the direction of each lattice vector.

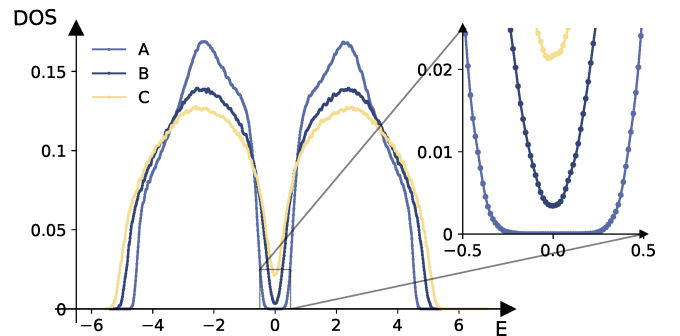


FIG. 4. Examples of DOS calculated for the points A,B,C marked in Fig. 1. The inset shows a zoom around the Fermi level which corresponds to $E = 0$ at half-filling. 20 disorder realizations were always performed and a system of 1024×1024 sites was considered.

finite-disorder Chern insulating phases with $C = \pm 1$ exist for any infinitesimal disorder. To understand if this is the case, we fixed $B = 0$ (QBC system for $W = 0$) and computed the Chern number as a function of W for different system sizes. The results are shown in Fig. 3, where it is clear that the $C = -1$ phase occurs for disorder strengths that approach $W = 0$ as the system size is increased. These results suggest that in the thermodynamic limit the $B = 0$ QBC point is unstable to the formation of the $C = -1$ phase for any infinitesimal disorder. The same is expected for the QBC point at $B = -2$ as suggested by the symmetry of the phase diagram around $B = -1$.

B. Gapped/Gapless Regions

In order to study the existence of a spectral gap at the Fermi level ($E = 0$ at half-filling) we computed the DOS using the kernel polynomial method implemented in Kite [28]. In Fig. 1 is present the gapped/gapless transitions. The system was considered gapped when the DOS at the

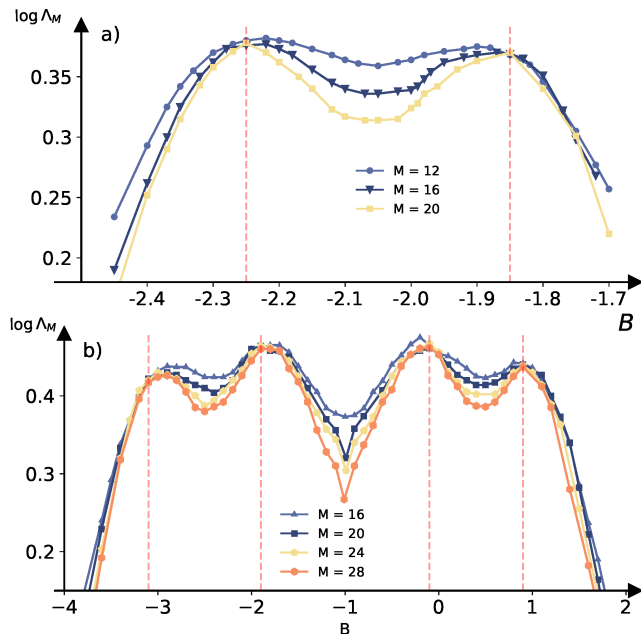


FIG. 5. Normalized localization length Λ_M as function of system transversal size M .

Fermi Level was below a certain threshold, ρ_{cut} , that was determined by exact diagonalization of the Hamiltonian in Eq. (5). In Appendix C we show the results that support our choice. The error in the transition from gapped to gapless corresponds to a variation of $\pm 25\%$ of that criterion. This error corresponds to the thickness of the gapped-gapless transition lines in Fig. 1. The small error shows that variations in the criterion do not affect significantly the results, especially in the regions of the topological phase transitions.

C. Localization

We studied the normalized localization length Λ_M obtained through the TMM, at the Fermi level ($E = 0$). Λ_M always decreases with M , except at specific points. This means that, as expected, all states at the Fermi level are localized except when a topological phase transition occurs accompanied by the merging of extended critical states carrying opposite Chern numbers. Example results are shown in Fig. 5. The results in Fig. 5(a) are for $W = 5$ and a range of B containing the $C = 2/C = 1$ and $C = 1/C = 0$ transitions. Fig. 5(b) corresponds to a cut at $W = 8$, for a range of B containing all the topological phase transitions. The phase transition points were considered to be those with constant Λ_M . The uncertainty in these points was considered to be the range of B over which there isn't an undoubtful decrease of Λ_M with M . This uncertainty is represented in Fig. 1 by the shaded red bars, being perfectly bounded by the error bars in

the Chern number.

IV. DISCUSSION

The phase diagram of the QBC system here unveiled shows many features that are characteristic of well-known disordered topological insulators [9–14, 16–19, 33–39], such as the existence of robust finite-disorder gapped and gapless topological insulating phases. However, there is a feature that distinguishes it from the previously explored models: the existence of new disorder-driven topological phases with $C = \pm 1$, absent in the clean limit. Our results suggest that the existence of a QBCP is a key ingredient for the formation of these phases. In particular, the finite-size scaling analysis in Fig. 3 is a strong indication that they are instabilities of the QBCPs: in the thermodynamic limit, any infinitesimal amount of disorder should drive the QBC system to one of these phases. Furthermore, from the phase diagram in Fig. 1, it is clear that for low disorder the new topological phases are located around the clean-limit QBCP.

The new phases with $C = \pm 1$ are also TAI since they can be reached by increasing disorder from a trivial phase. TAI phenomena were by now observed in a multitude of disordered topological insulators. However, there is an important difference from the conventional TAI in the present case: the $C = \pm 1$ TAI phases have a Chern number that does not exist in any zero-disorder topological phase of the model. Therefore, these TAI phases do not evolve smoothly from the clean-limit phases as disorder is increased, in contrast to conventional TAIs.

A possible variation of the QBC system is to split the QBCP into two Dirac cones with a suitable perturbation (see SM). Even in this case, a finite disorder gives rise to the $C = \pm 1$ phases which could be an argument against the importance of the QBCP for their existence. Nonetheless, the topological information carried by the split Dirac cones and the QBCP is the same since no gap is opened in the splitting process. The topological properties of the new system can then be traced back to the possibility of creating a QBCP without closing the gap.

Finally, the results obtained here are not restricted to disorder of the Anderson type. We also obtained the phase diagram for binary disorder, being qualitatively similar to the phase diagram for Anderson disorder (see SM).

V. CONCLUSIONS

We have studied a model of a QBC system under gap-opening and disorder-inducing couplings. A complete spectral, topological and localization analysis was carried out in order to obtain a detailed phase diagram. We not only found that the topological phases existing

in the clean limit were robust to disorder but also that new gapless topological phases were formed. Most importantly, we found a new instability of the QBCP: a disorder-induced instability to gapless topological phases with Chern numbers $C = \pm 1$, that are absent in the clean limit.

An interesting question for future work is whether instabilities of the QBCPs to electron-electron interactions can give rise to topological phases with similar properties to the gapless topological insulators here uncovered. The full phase diagram capturing the interplay between disorder and interactions would then be a natural follow-up.

Appendix A: Evolution of Phase Diagram with B_x constant perturbation

To study the robustness of the QBCP we introduce the term $\mathbf{b} \cdot \boldsymbol{\sigma}$ in the Hamiltonian written in the reciprocal space where \mathbf{b} can be a constant vector with three components, $\mathbf{b} = (b_x, b_y, b_z)$. The b_x perturbation lifts the degeneracy of the QBCP, splitting it into two Dirac Cones. In fig. 6, we show the value of the Chern number in the plane B vs b_x with increasing disorder. For a small b_x the phase diagram of the fig. 2 is practically unchanged. It is also clear from the figure that the $C = \pm 1$ phases exist even when $b_x \neq 0$.

Appendix B: Qualitative Phase Diagram for Binary Disorder

In this section, we present the phase diagram for binary disorder. In this case, the on-site potentials ϵ_i follow the following distribution:

$$P_V(\epsilon_i) = \frac{1}{2} (\delta(\epsilon_i) + \delta(V - \epsilon_i))$$

The Chern number results are shown in fig. 7. Qualitatively, the phase diagram is very similar to the one obtained for Anderson disorder in Fig. 1. In particular, the disorder-induced topological phases are still present and the reentrant TAI behaviour is also observed. However it is needed a smaller degree of disorder to destroy all the non-trivial phases. Besides this,, for large B (absolute value), the $C = \pm 1$ phases are much narrower with binary disorder which means that they are more robust to Anderson disorder.

Appendix C: Gapped/gapless regions

In this section, we present details on the criterion used in the main text to distinguish gapped and gapless regimes.

Due to the finite resolution of kernel polynomial methods (KPM), it is typically challenging to find the transition point between gapped and gapless regimes. In particular, the DOS obtained through KPM may have a finite spectral weight at energies within gaps. We therefore use finite-size scaling results from exact diagonalization to find a suitable ρ_{cut} below which the KPM DOS should be considered null. For the system to be gapless the difference between the states immediately above and under the Fermi level must converge to 0 in the thermodynamic limit. To define ρ_{cut} , we set the parameter $B = -1$. After fitting the finite-size scaling results to a cubic function and extrapolating to $N \rightarrow \infty$, we observe that for a disorder around $W \approx 4.2$ the system must be gapless. It was, then, just a matter of computing the DOS with Kite [28] for $B = -1$ and that critical disorder and then fix the $\rho(E = 0)$ to be the ρ_{cut} .

-
- [1] M. Z. Hasan and C. L. Kane, Rev. Mod. Phys. **82**, 3045 (2010).
 - [2] X.-L. Qi and S.-C. Zhang, Rev. Mod. Phys. **83**, 1057 (2011).
 - [3] B. A. B. with Taylor L. Hughes, *Topological Insulators and Topological Superconductors* (Princeton University Press, 2013).
 - [4] C.-K. K. Chiu, J. C. Y. Teo, A. P. Schnyder, and S. Ryu, Reviews of Modern Physics **88**, 035005 (2016).
 - [5] B. Wu, J. Song, J. Zhou, and H. Jiang, Chinese Physics B **25**, 117311 (2016), URL <https://doi.org/10.1088/1674-1056/25/11/117311>.
 - [6] A. Altland and M. R. Zirnbauer, Phys. Rev. B **55**, 1142 (1997).
 - [7] D. Xiao, M. C. Chang, and Q. Niu, Reviews of Modern Physics **82**, 1959 (2010).
 - [8] B. Kramer and A. MacKinnon, Rep. Prog. Phys. **56**, 1469 (1993).
 - [9] M. Onoda and N. Nagaosa, Phys. Rev. Lett. **90**, 206601 (2003).
 - [10] M. Onoda, Y. Avishai, and N. Nagaosa, Phys. Rev. Lett. **98**, 76802 (2007).
 - [11] E. V. Castro, M. P. López-Sancho, and M. A. Vozmediano, Physical Review B - Condensed Matter and Materials Physics **92** (2015).
 - [12] E. V. Castro, R. De Gail, M. P. López-Sancho, and M. A. Vozmediano, Physical Review B **93**, 245414 (2016).
 - [13] J. Li, R.-L. Chu, J. K. Jain, and S.-Q. Shen, Phys. Rev. Lett. **102**, 136806 (2009), URL <https://link.aps.org/doi/10.1103/PhysRevLett.102.136806>
 - [14] C. W. Groth, M. Wimmer, A. R. Akhmerov, J. Tworzydło, and C. W. Beenakker, Physical Review Letters **103** (2009).
 - [15] C. L. Kane and E. J. Mele, Physical Review Letters **95**, 226801 (2005).
 - [16] C. P. Orth, T. Sekera, C. Bruder, and T. L. Schmidt, Scientific Reports **6** (2016).
 - [17] J. Song, H. Liu, H. Jiang, Q. F. Sun, and X. C. Xie, Physical Review B - Condensed Matter and Materials Physics **85** (2012).

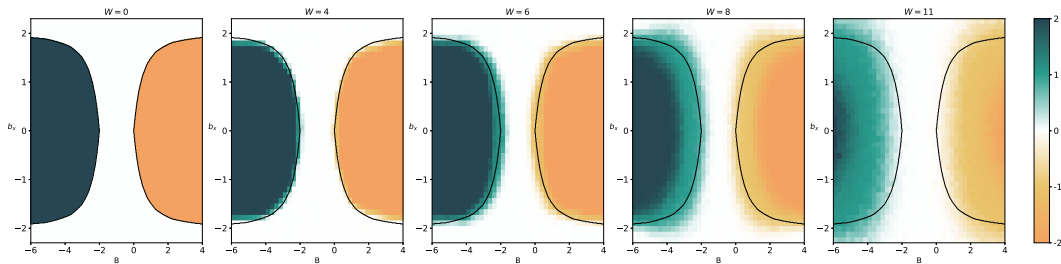


FIG. 6. Evolution of phase diagram in the $B - b_x$ plane. The black lines correspond to the phase transition for null disorder corresponding to the points where there are Dirac Cones or QBCPs in the spectrum. All points were averaged with 100 disorder configurations for systems of size 15×15 .

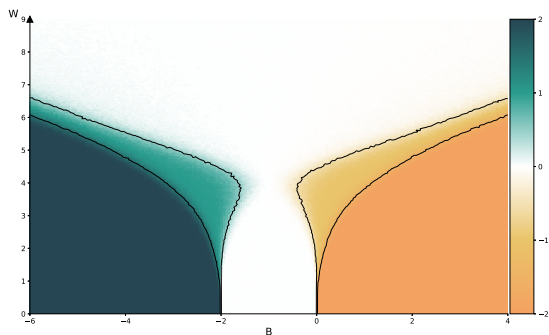


FIG. 7. Qualitative description of the phase diagram with Binary disorder. All points were averaged with 200 disorder configurations with systems of size 15×15

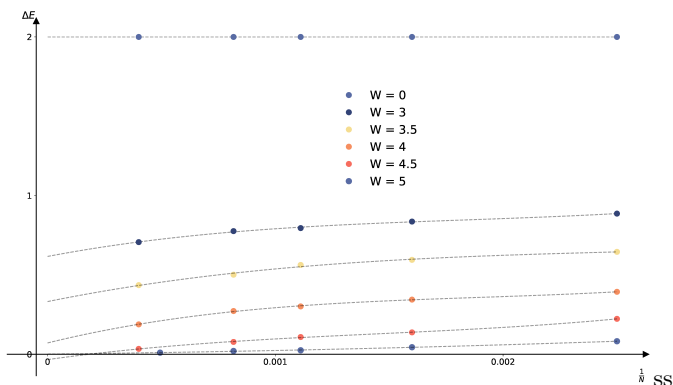


FIG. 8. Difference from the two states directly above and under the Fermi Level, computed using exact diagonalization for different systems with N sites.

- [18] J. H. García, L. Covaci, and T. G. Rappoport, *Physical Review Letters* **114**, 1 (2015).
- [19] M. Gonçalves, P. Ribeiro, and E. V. Castro, arXiv:1807.11247 (????), URL <http://arxiv.org/abs/1807.11247>.
- [20] K. Sun, H. Yao, E. Fradkin, and S. A. Kivelson, *Phys. Rev. Lett.* **103**, 46811 (2009), ISSN 00319007, 0905.0907.

- [21] S. Uebelacker and C. Honerkamp, *Phys. Rev. B* **84**, 205122 (2011).
- [22] J. M. Murray and O. Vafek, *Phys. Rev. B* **89**, 201110 (2014).
- [23] S. Ray, M. Vojta, and L. Janssen, *Phys. Rev. B* **98**, 245128 (2018), ISSN 2469-9950, 1810.07695, URL <http://arxiv.org/abs/1810.07695><http://dx.doi.org/10.1103/PhysRevB.98.245128>.
- [24] T. S. Zeng, W. Zhu, and D. Sheng, *npj Quantum Mater.* **3**, 49 (2018), ISSN 23974648, 1805.01101, URL <http://arxiv.org/abs/1805.01101><http://dx.doi.org/10.1038/s41535-018-0048-2>.
- [25] J. Wang, C. Ortix, J. van den Brink, and D. V. Efremov, *Phys. Rev. B* **96**, 201104 (2017), ISSN 2469-9950, 1710.09632, URL <http://arxiv.org/abs/1710.09632><http://dx.doi.org/10.1103/PhysRevB.96.201104>.
- [26] Y.-M. Dong, Y.-H. Zhai, D.-X. Zheng, and J. Wang, *Phys. Rev. B* **102**, 134204 (2020), URL <https://link.aps.org/doi/10.1103/PhysRevB.102.134204>.
- [27] F. D. M. Haldane, *Physical Review Letters* **61**, 2015 (1988).
- [28] S. M. João, M. Anđelković, L. Covaci, T. G. Rappoport, J. M. V. P. Lopes, and A. Ferreira, *R. Soc. Open Sci.* **7**, 191809 (2020), ISSN 2054-5703, 1910.05194, URL <http://arxiv.org/abs/1910.05194><http://dx.doi.org/10.1098/rsos.191809>.
- [29] T. Fukui, Y. Hatsugai, and H. Suzuki, *Journal of the Physical Society of Japan* **74**, 1674 (2005).
- [30] A. Mackinnon and B. Kramer, *Phys. Rev. Lett.* **47**, 1546 (1981).
- [31] A. MacKinnon and B. Kramer, *Zeitschrift für Physik B Condensed Matter* **53**, 1 (1983).
- [32] K. Hoffmann and M. Schreiber, *Computational Physics: Selected Methods Simple Exercises Serious Applications* (Springer Berlin Heidelberg, 2012).
- [33] G.-G. Liu, Y. Yang, X. Ren, H. Xue, X. Lin, Y.-H. Hu, H.-x. Sun, B. Peng, P. Zhou, Y. Chong, et al., *Phys. Rev. Lett.* **125**, 133603 (2020), URL <https://link.aps.org/doi/10.1103/PhysRevLett.125.133603>.
- [34] S. Stützer, Y. Plotnik, Y. Lumer, P. Titum, N. H. Lindner, M. Segev, M. C. Rechtsman, and A. Szameit, *Nature* **560**, 461 (2018), ISSN 1476-4687, URL <https://doi.org/10.1038/s41586-018-0418-2>.
- [35] J. Song, Y.-Y. Zhang, Y. Li, and Q. feng Sun, *Journal of Physics: Condensed Matter* **27**, 045601 (2015), URL <https://doi.org/10.1088/0953-8984/27/4/045601>.
- [36] Y. Su, Y. Avishai, and X. R. Wang, *Phys. Rev. B* **93**, 214206 (2016), URL <https://link.aps.org/doi/10.1103/PhysRevB.93.214206>.
- [37] Y. Kuno, *Phys. Rev. B* **100**, 054108 (2019), URL

- [38] <https://link.aps.org/doi/10.1103/PhysRevB.100.054108>[39] H.-B. Wu and J.-J. Liu, Phys. Rev. B **103**, 115430 (2021), URL <https://link.aps.org/doi/10.1103/PhysRevB.103.115430>.
- H.-C. Hsu and T.-W. Chen, Phys. Rev. B **102**, 205425 (2020), URL <https://link.aps.org/doi/10.1103/PhysRevB.102.205425>.